Biochemical Kinetic Characterization of the *Acanthamoeba* Myosin-I ATPase

E. Michael Ostap and Thomas D. Pollard

Department of Cell Biology and Anatomy, The Johns Hopkins University School of Medicine, Baltimore, Maryland 21205

Abstract. *Acanthamoeba* myosin-IA and myosin-IB are single-headed molecular motors that may play an important role in membrane-based motility. To better define the types of motility that myosin-IA and myosin-IB can support, we determined the rate constants for key steps on the myosin-I ATPase pathway using fluorescence stopped-flow, cold-chase, and rapid-quench techniques. We determined the rate constants for ATP binding, ATP hydrolysis, actomyosin-I dissociation, phosphate release, and ADP release. We also determined equilibrium constants for myosin-I binding to actin filaments, ADP binding to actomyosin-I, and ATP hydrolysis. These rate constants define an ATPase mechanism in which (*a*) ATP rapidly dissociates actomyosin-I, (*b*) the predominant steady-state intermediates are in a rapid equilibrium between actin-bound and free states, (*c*) phosphate release is rate limiting and regulated by heavy-chain phosphorylation, and (*d*) ADP release is fast. Thus, during steady-state ATP hydrolysis, myosin-I is weakly bound to the actin filament like skeletal muscle myosin-II and unlike the microtubule-based motor kinesin. Therefore, for myosin-I to support processive motility or cortical contraction, multiple myosin-I molecules must be specifically localized to a small region on a membrane or in the actin-rich cell cortex. This conclusion has important implications for the regulation of myosin-I via localization through the unique myosin-I tails. This is the first complete transient kinetic characterization of a member of the myosin superfamily, other than myosin-II, providing the opportunity to obtain insights about the evolution of all myosin isoforms.

Myosin-I is the single-headed low molecular weight member of the myosin superfamily that has been proposed to mediate actin-dependent membrane-based motility (for review see Pollard et al., 1991; Cheney et al., 1993). This membrane-based motility may include (*a*) the rearrangement of the actin-rich cell cortex, and (*b*) the movement of organelles and membranes along actin filaments. In vitro motility assays have shown that membrane-bound myosin-I supports ATP-dependent actin gliding. Localization and myosin-I knockout experiments suggest that unique myosin-I isoforms within a single cell may play specific roles in several actin-dependent membrane-based movements, including phagocytosis, pseudopod extension, contractile vacuole function, and directed organelle motility (Adams and Pollard, 1986; Doberstein et al., 1993; Jung et al., 1993; Titus et al., 1993; Baines et al., 1995). However, the precise molecular role and mechanism of myosin-I in these motile events has not been established.

To determine the function of myosin-I in membrane-based motility, one must first determine the biochemical and physical properties of the protein. Biochemical binding studies have demonstrated that *Acanthamoeba* myosin-I tails bind tightly to negatively charged membranes as well as to actin via a noncatalytic actin-binding site (Lynch et al., 1986; Miyata et al., 1989; Adams and Pollard, 1989; Doberstein and Pollard, 1992). Localization studies also suggest the binding of myosin-I to actin in the cell cortex and to specific membrane surfaces (Yonemura and Pollard, 1990; Baines et al., 1992; Baines et al., 1995). Measurements of the steady-state ATPase kinetics and actin binding of *Acanthamoeba* myosin-I indicate that myosin-I has actin-activated ATPase activity that is regulated by the phosphorylation of the myosin-I heavy chain (Pollard and Korn, 1972; Albanesi et al., 1983). While these measurements provide valuable steady-state information about the physical properties of the myosin-I, they do not provide the detailed chemical information that is necessary to define the biochemical and physical limitations of the enzyme.

To better define the types of motility that myosin-I can support, we have determined the rate and equilibrium constants for key steps on the *Acanthamoeba* myosin-IA (MIA)[1] and myosin-IB (MIB) ATPase cycle using tran-

Address all correspondence to E.M. Ostap, Department of Cell Biology and Anatomy, Johns Hopkins University School of Medicine, 725 N. Wolfe Street, Baltimore, MD 21205. Tel.: (410) 955-5672. Fax: (410) 955-4129. e-mail: mostap@welchlink.welch.jhu.edu

1. *Abbreviations used in this paper*: mant-ATP, *N*-methyanthraniloyl-ATP; MHCK, myosin-I heavy-chain kinase; MIA, myosin-IA; MIB, myosin-IB.

sient kinetic techniques. The biochemistry of myosin-I ultimately defines what myosin-I can do; therefore, determination of the biochemical rate constants allows us to (*a*) understand how myosin-I interacts with actin and ATP to support the motility that has been observed, (*b*) put physical limits on the myosin-I–based motility that has been proposed, (*c*) understand how *Acanthamoeba* myosin-I is regulated by heavy-chain phosphorylation, and (*d*) determine if different myosin-I isoforms within a single cell type have unique enzymatic properties that are most suitable for specialized cell functions.

This is the first complete biochemical characterization of a member of the myosin superfamily, other than myosin-II. Therefore, this is the first opportunity to obtain insights about the evolution of all the myosin isoforms by comparing both the myosin sequences and the biochemical kinetics.

Materials and Methods

Preparations and Solutions

Acanthamoeba castellanii (Neff strain) myosin-IA, myosin-IB, myosin-IC, and myosin-I heavy-chain kinase (MHCK) were prepared as described by Lynch et al. (1991). Myosin-I was stored for up to 3 wk at −20°C in 10 mM Tris, pH 7.5, 100 mM KCl, 1 mM DTT, 0.01% NaN_3, and 50% glycerol (storage buffer). MHCK was stored at −20°C in 20 mM Tris, pH 7.5, 50 mM KCl, 1 mM DTT, 0.01% NaN_3, and 50% glycerol.

Before use, myosin-I was (*a*) dialyzed against assay buffer (25 mM Tris, pH 7.5, 100 mM KCl, 2 mM $MgCl_2$, 1 mM EGTA, 1 mM DTT), or (*b*) eluted from a 10-ml G-25 spin column that was equilibrated in assay buffer. The myosin-I concentration was determined using the bicinchonic acid protein assay (Pierce Chemical Co., Rockford, IL) using BSA or rabbit skeletal myosin subfragment-1 as a standard.

After phosphorylation by MHCK (Lynch et al., 1991), the myosin-I was dialyzed against Q-buffer (25 mM Tris, pH 8.8, 100 mM KCl, 1 mM DTT) and loaded on to a mono-Q column (Pharmacia Biotech, Piscataway, NJ). The myosin-I was eluted with a 0.1–0.5 M KCl gradient in Q-buffer. Myosin-I was then dialyzed against storage or assay buffer. The repurification of myosin-I after phosphorylation was necessary to remove MHCK and nucleotides. Phosphorylation of the myosin heavy chain was >80% as determined by radioactive counting of myosin-I phosphorylated with [γ-^{32}P]-ATP that was excised from an SDS–polyacrylamide gel. Phosphorylated myosin-I supported the gliding of actin filaments in the in vitro motility assay (Zot et al., 1992; data not shown). The steady-state ATPase rates of phosphorylated MIA and MIB were determined in low ionic strength buffer (2 mM ATP, 2 mM $MgCl_2$, 1 mM EGTA, 5 mM KCl, 1 mM DTT, 15 mM imidazole, pH 7.5) in the presence of 75 μM actin as described by Pollard (1982). The actin-activated ATPase rate of MIA = 7 s^{-1} and MIB = 6 s^{-1}. These rates are similar to those reported previously by Albanesi et al. (1985).

Rabbit skeletal muscle actin was prepared as described (Spudich and Watt, 1971). Actin was labeled with pyrenyl iodoacetamide to the extent of >0.95 pyrene/actin and gel filtered as described (Pollard, 1984).

Nucleotide concentrations were determined spectrophotometrically after each dilution and before each experiment by absorbance at 259 nm, using an extinction coefficient of 15,400 M^{-1} cm^{-1}. *N*-methyanthraniloyl-ATP (mant-ATP) (Hiratsuka, 1983) was generously provided by Dr. E.W. Taylor (University of Chicago, Chicago, IL). Mant-ATP concentrations were determined spectrophotometrically at 255 nm, using an extinction coefficient of 23,300 M^{-1} cm^{-1} (Hiratsuka, 1983).

Fluorescence Titrations

Fluorescence titrations were performed at 22°C using a fluorimeter (Alphascan; Photon Technology Intl., South Brunswick, NJ). Pyrene-actin was excited at 365 nm (2-nm half-width), and the emission spectrum was scanned from 375 to 450 nm. The peak intensity at 405 nm was used in the titration analysis.

Data obtained from the steady-state titrations were fitted by using a nonlinear least-squares fit (Press et al., 1986) to the following equation:

$$\alpha = (2A)^{-1} \; [-A-M-K_d + (A^2 - 2AM + 2AK_d + M^2 + 2MK + K_d^2)^{1/2}] \quad (1)$$

where A is the total actin concentration, M is the total myosin-I concentration, K_d is the dissociation constant, and α is the fractional saturation of actin by myosin-I (Geeves and Jeffries, 1988). α is defined in terms of the fluorescence signal (F) as:

$$\alpha = (F_o - F)/(F_o - F_\infty) \quad (2)$$

where F_o is the fluorescence signal in the absence of myosin-I, and F_∞ is the fluorescence signal at infinite myosin-I concentrations (Geeves and Jeffries, 1988).

Transient Kinetics

A stopped-flow apparatus modeled after a design by Johnson (1986) and described by Sinard and Pollard (1990) was used to acquire all transient fluorescence data. The dead time of the instrument is <3 ms with a 100-μl sample volume. Fluorescence excitation was provided by a 100-W Hg lamp filtered with a 365-nm band-pass filter, and emission was monitored at 90° through a 410-nm long-pass filter. The data was digitized and transferred to an IBM-compatible computer for analysis.

Cold-chase and rapid-quench experiments were performed at 22°C using the chemical quench-flow (RQF-3; KinTek Instruments, State College, PA) in the laboratory of Michael W. Washabaugh (Johns Hopkins University, Baltimore, MD). For each time point, myosin-I was loaded into one sample loop (35 μl), and [γ-^{32}P]ATP was loaded into the second loop (35 μl). The reactants were rapidly mixed and pushed into a reaction loop. After a specified time, the reaction was either (*a*) chased with 2.5 mM ATP and then quenched after 2 min with 2 M HCl, 0.35 mM NaH_2PO_4, or (*b*) quenched with 2 M HCl, 0.35 mM NaH_2PO_4. Free ^{32}P was separated from ATP and quantitated by the activated charcoal method (White and Rayment, 1993).

Stopped-flow and rapid-quench data were fitted to exponentials by a nonlinear least-squares curve fit using the Marquardt method (Press et al., 1986). All concentrations refer to the concentrations of the reactants after mixing.

Results

Mant-ATP Binding to Myosin-I

We used the increase in the fluorescence of the nucleotide analogue mant-ATP (Hiratsuka, 1983) to measure the rate of nucleotide binding to MIA and MIB. Under pseudo–first-order conditions in stopped-flow experiments (Fig. 1), the fluorescence increase at each nucleotide concentration tested (1–20 μM) fit a single exponential, and the rate increased linearly with mant-ATP concentration up to the highest practical concentration. At all concentrations the rate of mant-ATP binding to MIB was significantly faster than the rate of binding to MIA.

The mechanism for mant-ATP binding to myosin-I can be defined as:

$$\text{mant-ATP} + \text{M} \underset{}{\overset{K_1}{\leftrightarrow}} \text{M(mant-ATP)} \overset{k_2}{\rightarrow} \text{M.mant-ATP**} \quad (3)$$

where step 1 is the formation of a binary collision complex, and step 2 is a rapid myosin isomerization that leads to the increased fluorescence of the nucleotide (mant-ATP**). The slope of a plot of the observed rate constant vs. the nucleotide concentration (Fig. 2) gives the apparent second-order rate constant (K_1k_2), which is 0.74 $\mu M^{-1}s^{-1}$ for unphosphorylated MIA and 3.37 $\mu M^{-1}s^{-1}$ for MIB (Table I). Phosphorylated MIA and MIB bound mant-ATP at the same rate as unphosphorylated myosin-I (Fig. 2; Table I). We could not evaluate the first-order rate constant for

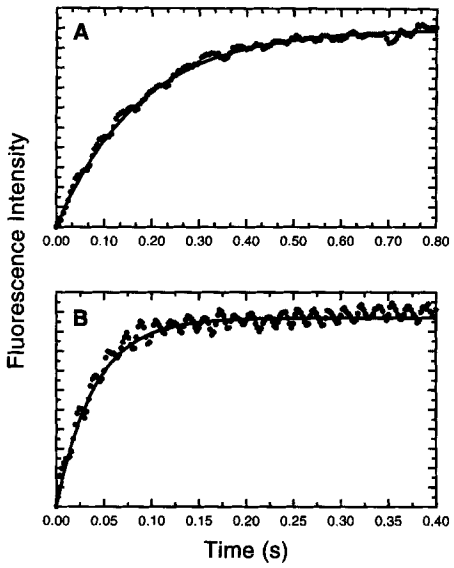

Figure 1. Stopped-flow fluorescence transients showing the binding of 9 μm mant-ATP to (*A*) 0.5 μm myosin-IA and (*B*) 0.5 μM myosin-IB. The solid lines are single exponential fits to the fluorescence data with rates of (*A*) 5.7 s^{-1} and (*B*) 25 s^{-1}. Conditions: 100 mM KCl, 2 mM $MgCl_2$, 1 mM EGTA, 1 mM DTT, 25 mM Tris, pH 7.5.

isomerization, k_2, directly because of the low signal-to-noise ratio of the fluorescence transient at mant-ATP concentrations >30 μM.

Myosin-I Binding to Pyrene-Actin

The 50–60% fluorescence quenching upon myosin-I binding to pyrene-actin allowed us to monitor association and dissociation of the actomyosin-I complex (Geeves and Jeffries, 1988; Richie et al., 1993). The fluorescence signal from the equilibrium binding of MIA or MIB to 0.5 μM pyrene-actin-phalloidin in the absence of ATP was normalized to the maximum fluorescence intensity (Fig. 3). A

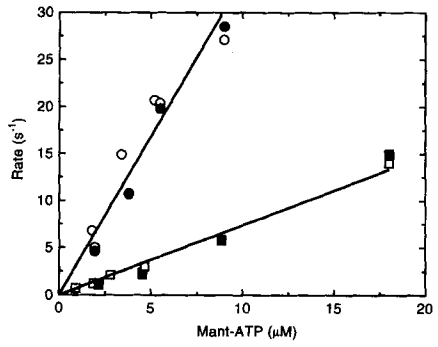

Figure 2. Rate of binding of mant-ATP to (*open symbols*) unphosphorylated and (*closed symbols*) phosphorylated (*squares*) myosin-IA and (*circles*) myosin-IB as a function of nucleotide concentration. The observed first-order rate constants were obtained by fitting the stopped-flow data at each nucleotide concentration to a single exponential. The solid lines are the best linear fits through the unphosphorylated data points. K_1k_2 = 0.74 $\mu M^{-1}s^{-1}$ for myosin-IA. K_1k_2 = 3.37 $\mu M^{-1}s^{-1}$ for myosin-IB. These values were the same for phosphorylated and unphosphorylated myosin-I.

Table I. Summary of Myosin-IA and Myosin-IB Rate and Equilibrium Constants

Rate constant	MIA	MIB
K_1k_2	0.74 $\mu M^{-1}s^{-1}$	3.37 $\mu M^{-1}s^{-1}$
$K_1'k_2'$	0.29 $\mu M^{-1}s^{-1}$	1.3 $\mu M^{-1}s^{-1}$
k_2'	>300 s^{-1}	>300 s^{-1}
$k_{+3} + k_{-3}$	≥16 s^{-1}	≥53s^{-1}
K_3	1.9	1.5
k_5'	ND	>80 s^{-1}
K_5'	1.1 × 10^4 M^{-1}	1.9 × 10^4 M^{-1}
K_6	1.7 × 10^7 M^{-1}	2.0 × 10^7 M^{-1}

Phosphorylation of the myosin-I heavy chain does not affect these rate constants.

nonlinear least-squares fit to the data yields a dissociation equilibrium constant ($1/K_6$) of 0.06 μM for MIA and 0.05 μM for MIB (unphosphorylated; Table I). These values are comparable to those obtained under similar conditions for skeletal muscle myosin-II and myosin-II from *Dictyostelium* (Ritchie et al., 1993).

ATP-induced Dissociation of Pyrene–Actomyosin-I

Addition of ATP to pyrene–actomyosin-IA or -IB increased the fluorescence to that of pyrene-actin alone. This recovery of fluorescence indicates that (*a*) the ATP-sensitive strong-binding site on MIA or MIB completely dissociates from the actin within the limits of detection of this assay, and (*b*) the pyrene signal does not report the attachment of the ATP-insensitive actin-binding site on MIA or MIB (Lynch et al., 1986).

The time-course of ATP-induced dissociation of MIA or MIB from pyrene-actin-phalloidin by ATP is best fit to a single exponential at all concentrations tested (Fig. 4). Like the reaction with mant-ATP, the transient at 10 μM ATP is significantly slower with MIA (4.1 s^{-1}) than MIB (16 s^{-1}), consistent with a slower rate of ATP binding to MIA.

The rate of actomyosin-I dissociation increased linearly with the ATP concentration under pseudo–first-order conditions (Fig. 5). The mechanism for actomyosin-I dissociation can be defined as:

$$\text{ATP} + \text{AM} \overset{K_1'}{\leftrightarrow} \text{AM(ATP)} \overset{k_2'}{\rightarrow} \text{AM.ATP} \overset{k_8}{\leftrightarrow} \text{A**} + \text{M.ATP} \quad (4)$$

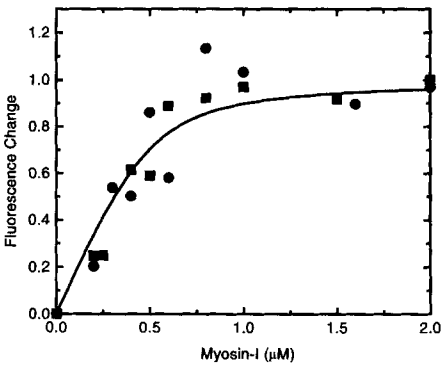

Figure 3. Fluorescence titration of 0.5 μM pyrene-actin-phalloidin with (*squares*) myosin-IA and (*circles*) myosin-IB. Maximum quenching of fluorescence by myosin-I is plotted as 1.0. The solid line is the best fit to the myosin-IA data as described in the Materials and Methods. K_d = 0.06 μM for myosin-IA and myosin-IB.

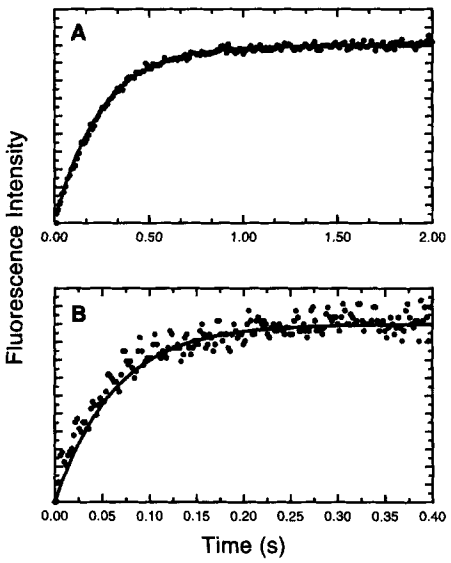

Figure 4. Stopped-flow fluorescence transients showing the dissociation of 0.5 μM unphosphorylated (*A*) myosin-IA and (*B*) myosin-IB from 0.5 μM pyrene-actin-phalloidin by 10 μM ATP. The solid lines are single exponential fits to the fluorescence data with rates of (*A*) 4.1 s^{-1} and (*B*) 16 s^{-1}.

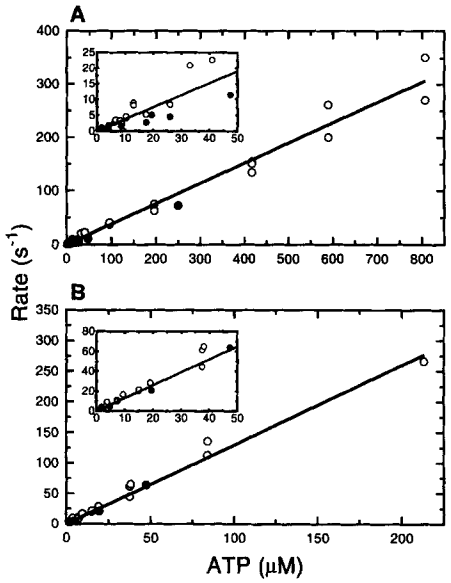

Figure 5. Rate of ATP-induced dissociation of (*open symbols*) unphosphorylated and (*closed symbols*) phosphorylated (*A*) myosin-IA and (*B*) myosin-IB from pyrene-actin-phalloidin as a function of nucleotide concentration. The observed first-order rate constants were obtained at each nucleotide concentration by fitting the stopped-flow data to a single exponential. The solid lines are the best linear fits through the unphosphorylated data points. $K_1k_2 = 0.29$ μM^{-1} s^{-1} for myosin-IA. $K_1k_2 = 1.3$ μM^{-1} s^{-1} for myosin-IB. The values for phosphorylated myosin-I were not significantly different. The insets show the data points at low nucleotide concentrations.

where step 1 is a rapid equilibrium, step 2 is a rate-limiting isomerization that precedes rapid dissociation (k_8), and A** is the high fluorescence state of actin. The apparent second-order rate constant ($K_1'k_2'$) can be obtained from the slopes of the curves in Fig. 5: $K_1'k_2' = 0.29$ $\mu M^{-1}s^{-1}$ for MIA and $K_1'k_2' = 1.3$ $\mu M^{-1}s^{-1}$ for MIB (Table I). The apparent second-order rate constant for myosin-IC is 0.60 $\mu M^{-1}s^{-1}$ (data not shown). Phosphorylation of MIA and MIB did not significantly change the apparent second-order rate constants (Fig. 5; Table I).

At high nucleotide concentrations, the maximum rate of actomyosin-I dissociation should be limited by k_2', resulting in a hyperbolic relationship between k_{obs} and the ATP concentration (Ma and Taylor, 1994). However, the low protein concentrations and the dead time of the stopped-flow instrument made measurements of >500 s^{-1} unattainable. The highest rate obtained for MIA or MIB was 300 s^{-1} (Table I). If the value of K_1' is assumed to be 500 M^{-1}, as determined for skeletal muscle and *Dictyostelium* cytoplasmic myosin-II (Ritchie et al., 1993), k_2' can be calculated from the apparent second-order rate constants (Table I): $k_2' = 580$ s^{-1} for MIA, and $k_2' = 2600$ s^{-1} for MIB. These rates for the dissociation of MI-ATP from actin are more than 50 times greater than the turnover number determined by steady-state ATPases at low ionic strength.

Cold-chase and Rapid-quench Kinetics

We studied the kinetics of ATP hydrolysis with cold-chase and rapid-quench experiments. The cold-chase experiments were performed to normalize the rapid-quench data to the number of active sites in the preparation and to determine the rate of ATP binding. The mechanism for ATP binding and hydrolysis can be defined as:

$$\mathrm{ATP} + \mathrm{M} \overset{K_1}{\leftrightarrow} \mathrm{M(ATP)} \overset{k_2}{\rightarrow} \mathrm{M.ATP} \overset{k_3}{\leftrightarrow} \mathrm{M.ADP.P_i} \overset{k_{slow}}{\rightarrow} \mathrm{M} + \mathrm{ADP} + \mathrm{P} \quad (5)$$

where K_1 and k_2 are the same as defined in the mant-ATP experiments, step 3 is ATP hydrolysis ($k_{+3} + k_{-3}$), and k_{slow} is the rate-limiting product release. The pseudo–first-order binding reaction of 25 μM ATP with 1 μM MIA (active sites) fit a single exponential with a rate of 25 s^{-1} and the reaction of 25 μM ATP with 1 μM MIB (active sites) fit a single exponential with a rate of 89 s^{-1} (Fig. 6; Table I). These rates give apparent second-order binding constants (K_1k_2) that agree very well with the apparent second-order rate constants determined by the mant-ATP stopped-flow experiments (Fig. 2; Table I). The large amplitude of the cold-chase curves also indicates that nearly all of the ATP that binds to the myosin-I is committed to the ATP hydrolysis cycle. Therefore, k_{-2} must be small.

Rapid-quench experiments report the rate of ATP hydrolysis and the number of ATPs hydrolyzed per active site (Fig. 6). The MIA and MIB rapid-quench data clearly show a rapid burst phase of ATP hydrolysis, followed by a slow phase that looks like a plateau on the rapid time scale of the experiment. The presence of the burst phase indicates that ATP hydrolysis ($k_{+3} + k_{-3}$) precedes the rate-limiting step (k_{slow}).

In the presence of 25 μM ATP, the rate of the MIA phosphate burst fits a single exponential with the rate of 16 s^{-1}, and the rate of the MIB phosphate burst fits a single exponential with the rate of 53 s^{-1}. At the low nucle-

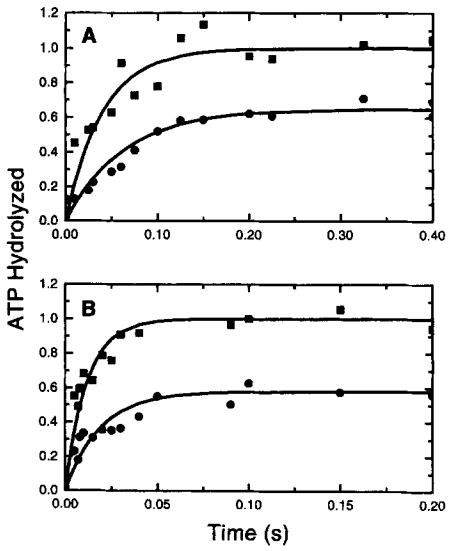

Figure 6. Transient binding and hydrolysis of 25 μM ATP by (*A*) 1 μM myosin-IA and (*B*) 1 μM myosin-IB (unphosphorylated) measured by (*squares*) cold-chase and (*circles*) rapid-quench experiments. The data was normalized to the plateau of the cold-chase experiments to correct for the myosin-I active site concentration (see Results). The solid lines are the best fits to the data.

otide concentrations used in these experiments, the rate of ATP hydrolysis ($k_{+3} + k_{-3}$) is limited by the rate of nucleotide binding (Table I), but even at these low ATP concentrations and in the absence of actin, ATP hydrolysis is faster than the maximum turnover rate at high actin concentrations.

The equilibrium constant for ATP hydrolysis can be obtained from the amplitude of the phosphate burst (*B*) if k_{slow} is rate limiting, and k_2 is essentially irreversible by the following relationship (Johnson and Taylor, 1978):

$$B = (K_3)/(1 + K_3) \tag{6}$$

The burst obtained from the MIA rapid-quench experiment is 0.65, which gives an equilibrium constant of K_3 = 1.9 (Table I). The burst obtained from the MIB rapid-quench experiments is 0.60, which gives an equilibrium constant of K_3 = 1.5 (Table I).

ADP Binding and Dissociation

The binding of ADP to pyrene–actomyosin-I was measured by competitive binding with ATP as described by:

$$\text{AM.ADP} \overset{K_5'}{\leftrightarrow} \text{AM} + \text{ATP} \overset{K_1'}{\leftrightarrow} \text{AM(ATP)} \overset{k_2'}{\rightarrow} \text{A**} + \text{M.ATP} \tag{7}$$

0.5 μM pyrene–actomyosin-I was incubated with varying concentrations of ADP and mixed with 40 μM ATP in a stopped-flow experiment (Fig. 7). MIA.ADP and MIB.ADP are strongly bound to the pyrene-actin before mixing as determined by the pyrene fluorescence. The time course of the fluorescence increase due to the ATP-induced dissociation of the actomyosin-I complex was fit to a single exponential and plotted vs. the ADP concentration. The rate of actomyosin-I dissociation (k_{obs}) was related to the ADP concentration by:

$$k_{obs} = k_0/\{1 + ([\text{ADP}]/K_d)\} \tag{8}$$

where k_{obs} is the observed dissociation rate, k_0 is the dissociation rate in the absence of ADP, and K_d is dissociation equilibrium constant for ADP (Geeves, 1989; Ma and Taylor, 1994). Nonlinear least-square fits to the data yield K_d values of 93 μM for MIA and 53 μM for MIB (Table I). Rates with phosphorylated MIA and MIB are not significantly different from those with unphosphorylated myosin-I (data not shown).

To determine if the ADP dissociation step measured in Fig. 7 is rate limiting, 250 μM ADP was incubated with pyrene-actin–MIB (unphosphorylated) and rapidly mixed with 500 μM ATP. This concentration of ADP should saturate the myosin-I active sites and should make the rate of ATP binding and actomyosin-I dissociation limited by the rate of ADP dissociation. The fluorescence increase with MIB fit a single exponential with a rate of 84 s^{-1}. This rate is significantly greater than the steady-state turnover number at low ionic strength (Albanesi et al., 1983), and is consistent with the relationship for competitive binding in a rapid equilibrium as defined above.

Discussion

In the following sections we first detail the interpretation of the kinetics experiments that form the basis of the proposed mechanism (Eq. 9). Then we compare this mechanism with those of skeletal myosin-II and kinesin, identify the step in the mechanism regulated by heavy-chain phosphorylation, and speculate on the biological consequences of the mechanism.

$$\begin{array}{ccccccccccc} & & k_1' & & k_2' & & k_3' & & k_4' & & k_5' \\ \text{AM} & \leftrightarrow & \text{AM(ATP)} & \leftrightarrow & \text{AM.ATP} & \leftrightarrow & \text{AM.ADP.P}_i & \leftrightarrow & \text{AM.ADP} & \leftrightarrow & \text{AM} \\ K_6\Updownarrow & & K_7\Updownarrow & & K_8\Updownarrow & & K_9\Updownarrow & & K_{10}\Updownarrow & & K_6\Updownarrow \\ \text{M} & \leftrightarrow & \text{M(ATP)} & \leftrightarrow & \text{M.ATP} & \leftrightarrow & \text{M.ADP.P}_i & \leftrightarrow & \text{M.ADP} & \leftrightarrow & \text{M} \\ & & k_1 & & k_2 & & k_3 & & k_4 & & k_5 \end{array} \tag{9}$$

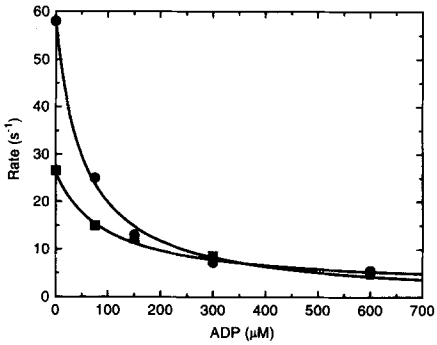

Figure 7. Dependence of the rate of 40 μM ATP binding to a 0.5 μM complex of pyrene-actin-phalloidin and (*squares*) myosin-IA or (*circles*) myosin-IB on the concentration of ADP. The observed first-order rate constants at each ADP concentration were obtained by fitting the stopped-flow data to a single exponential. The solid lines are the best fit of the data to obtain the dissociation constant for ADP (see Results). For pyrene–actomyosin-IA, K_d = 95 μM. For pyrene–actomyosin-IB, K_d = 53 μM. Phosphorylation of myosin-I did not significantly change these binding constants.

Interpretation of the Kinetics Experiments in Terms of a Mechanism for the Actomyosin-I ATPase Cycle

The experiments provide enough information to propose a complete chemical mechanism for the actomyosin-I ATPase cycle (Eq. 9). The binding of ATP to MIA and MIB is fast ($K_1'k_2'$). The apparent second-order rate constants determined from the mant-ATP experiments (Fig. 2; Table I) indicate that MIA and MIB bind ATP at rates of $>700\ s^{-1}$, assuming a cellular ATP concentration of 1 mM. This rate is ~100× faster than the rate-limiting step as determined from the turnover number. The ATP-induced dissociation of MIA and MIB from actin ($K_1'k_2'$), measured by pyrene-actin fluorescence (Fig. 5; Table I), is also much faster ($>300\ s^{-1}$) than the rate-limiting step, and may be limited by the rate of ATP binding at cellular ATP concentrations. Therefore, in the presence of actin, weakly bound (AM.ATP) and actin-detached (M.ATP) biochemical states of myosin-I are rapidly populated upon ATP binding.

We obtained the lower limits for the rates of ATP hydrolysis ($k_{+3} + k_{-3}$) by MIA ($\geq 16\ s^{-1}$) and MIB ($\geq 53\ s^{-1}$) using rapid-quench and cold-chase kinetics (Fig. 6). The presence of a phosphate burst (Fig. 6) shows that ATP hydrolysis occurs before the rate-limiting step in the absence of actin. The lower limits for the ATP hydrolysis rates are also greater than the turnover number of phosphorylated MIA and MIB in the presence of actin at low ionic strength.

The quench-flow experiments indicate that the equilibrium constants for ATP hydrolysis by MIA and MIB are >1. Addition of ATP to pyrene–actomyosin-IA or -IB increased the fluorescence to that of pyrene-actin alone indicating that the predominant steady-state intermediates are not strongly bound to the actin. Therefore, in the presence of actin, the weakly bound (AM.ADP.P_i) and the actin-detached (M.ADP.P_i) biochemical states are the most likely predominant steady-state intermediates.

From the nucleotide competition experiments (Fig. 7), we modeled ADP dissociation (k_5') as a rapid equilibrium step (Table I). The rate of ADP release at physiological ADP concentrations does not limit the steady-state turnover of ATP.

Because all of the rate constants that we determined are significantly faster than the steady-state ATPase rate, we can identify the step or steps between ATP hydrolysis and ADP release as the rate-determining transitions. The most likely candidates for this slow step are phosphate release (k_4'), or an isomerization preceding phosphate release. Phosphate release has been proposed to regulate the transition between the weak-binding (non–force-bearing) and strong-binding (force-bearing) states in the skeletal muscle myosin-II ATPase cycle (Eisenberg and Greene, 1980). The predominant actin-associated steady-state intermediates under these conditions would be the weak-binding AM.ATP and AM.ADP.P_i states. In the myosin-II ATPase cycle, these states are characterized by (*a*) a rapid equilibrium between actin-attached and actin-detached states (k_8, $k_9 > 1000\ s^{-1}$), and (*b*) relatively low affinity actin binding constants at physiological ionic strengths (K_{-8}, K_{-9} = 0.1–1.0 mM; for review see Bagshaw, 1993). These binding constants are similar to those obtained for myosin-IA (Lynch et al., 1986). The predominance of weak-binding intermediates significantly limits the types of motility that myosin-I can support (see below).

A second candidate for the rate-limiting step is an isomerization that has been proposed to occur after phosphate release and immediately before ADP release (Taylor, 1991). The significance of this alternative is that the predominant steady-state intermediate would be the strong-binding AM.ADP′ state (not shown). However, this possibility is unlikely in the case of myosin-I, because centrifuge binding assays indicate that the nucleotide-sensitive binding of MIA to actin is weak at low ionic strength compared to rigor binding, and the binding constant is not changed significantly by phosphorylation of the heavy chain (Lynch et al., 1986). Direct measurement of the ADP isomerization step (Taylor, 1991) could not be performed with MIA or MIB, because of the low ionic strength and high protein concentrations required. Myosin-I aggregates in solution under these conditions. It will be important to determine the rate and equilibrium constant for the pre-ADP release isomerization step to rule out this possibility.

Comparison with the Actomyosin-II ATPase Cycle

The rates of ATP binding and actomyosin-I dissociation are similar to those of skeletal, smooth, and cytoplasmic myosin-II (Marston and Taylor, 1980; Ritchie et al., 1993). The rate constant for actomyosin-IA dissociation is more like that for vertebrate slow muscle myosin-II, and the rate of actomyosin-IB dissociation is more like that for fast skeletal muscle myosin-II. These small but significant differences provide a biochemical rationale for the differential localization of the myosin-I isoforms to the cytoplasm, plasma membrane, or organelle membranes (Baines et al., 1995) where they may have different functions that require slightly different ATPase cycles for optimal activity, just like the muscle myosin-II isoforms expressed in physiologically different muscles (Marston and Taylor, 1980).

The rapid hydrolysis of ATP and the phosphate burst are also similar to the kinetic mechanism of myosin-II. The rate of ATP hydrolysis by skeletal myosin-II, measured directly by rapid quench, is $>100\ s^{-1}$ (Johnson and Taylor, 1978), and the rate of ATP hydrolysis by *Dictyostelium* myosin-II, measured indirectly by intrinsic tryptophan fluorescence, is $24\ s^{-1}$ (Ritchie et al., 1993). Even at the low ATP concentrations that we used (which limit the overall rate of the measured reaction), the hydrolysis rate is $>50\ s^{-1}$ for MIB and $>16\ s^{-1}$ for MIA, so the hydrolysis rates by the myosin-I isoforms are in the same range as skeletal muscle myosin-II. The equilibrium constants calculated from the burst amplitudes (Table I) are smaller than those determined for myosin-II under similar conditions ($K_3 > 9$ for skeletal myosin), but they still favor the post-ATP hydrolysis products. This results in a larger fraction of the myosin-I in the M.ATP state even at rates of ATP turnover in the presence of high actin concentrations.

ADP release (k_5') has been modeled as a rapid equilibrium step for skeletal (Ma and Taylor, 1994) and cytoplasmic myosin-II (Ritchie et al., 1993) with K_d's of 120 μM and 94 μM, respectively. These dissociation equilibrium constants are similar to those in this study (Table I). The actual rate of ADP release for skeletal myosin-II is 300–400 s^{-1}, and the isomerization step that precedes ADP release is 150–200 s^{-1} (Taylor, 1991). If the MIA and MIB

rate constants for the isomerization step are similar to myosin-II, the ADP release steps are not rate limiting.

An isomerization immediately before phosphate release determines the steady-state ATPase rate in unloaded skeletal muscle (k_4'; Ma and Taylor, 1993). This isomerization is the transition between the weak-binding and strong-binding intermediates. It is likely that this same step limits the actomyosin-I steady-state ATPase rate. Therefore, the kinetic mechanism of myosin-II with rapid detachment, ATP hydrolysis, reattachment, and product release adequately describes the mechanism for myosin-I.

Regulation of Myosin-I by Heavy-Chain Phosphorylation

Phosphorylation of myosin-I by MHCK increases the actin-activated steady-state ATPase rate >20-fold (Pollard and Korn, 1972; Albanesi et al., 1983) and may regulate myosin-I activity in vivo (Baines et al., 1995). The phosphorylation of MIA or MIB most likely regulates the rate-limiting phosphate release step (k_4'), since it did not change any of the rate or binding constants measured in this study (Table I). Since phosphorylation does not significantly alter the binding of MIA to actin in the presence of ATP (Lynch et al., 1986), phosphorylation does not change the equilibrium constant for the binding of actin to M.ATP and M.ADP.P_i or ADP release. Therefore, regulation must occur between the ATP hydrolysis step and ADP release, and most likely at the transition between the weak-binding (AM.ADP.P_i) and strong-binding (AM.ADP) states, which is phosphate release. This is the step that is regulated in skeletal muscle by the calcium activation of troponin and tropomyosin (Chalovich and Eisenberg, 1982).

MHCK phosphorylates MIA on a threonine and MIB on a serine, adding a negative charge to a neutral side chain (Brzeska et al., 1989). In myosins that do not require heavy-chain phosphorylation for activation, the corresponding residue is glutamate or aspartate on a flexible loop (residues 405–415 in chicken skeletal muscle) that has been proposed to interact directly with actin (Bement and Mooseker; 1995; Rayment et al., 1993). Therefore, our results suggest that the interaction between a negative charge on this loop and actin is essential for the activation of the ATPase activity for all myosins. Because heavy-chain phosphorylation regulates the same kinetic step that is regulated by thin filament activation, our results also suggest that the interaction of this loop with actin in skeletal muscle may be sterically regulated by tropomyosin as suggested by the atomic model for actomyosin and low angle x-ray diffraction of actin-tropomyosin (Holmes, 1995).

Relevance of Myosin-I Kinetics to In Vivo Function

Myosin-I spends most of the time during the ATPase cycle weakly bound to or detached from the actin filament. This is referred to as a small duty cycle. Therefore, a small number of myosin-I molecules is unlikely to support cortical contraction or the processive movement of molecular cargo over long distances. In contrast, the biochemical kinetics of the kinesin-microtubule ATPase cycle indicates that kinesin spends most of its time strongly bound to the microtubule (large duty cycle), preventing the dissociation of the kinesin (and cargo) from the microtubule and allowing processive movement powered by as few as one double-headed kinesin molecule (Romberg and Vale, 1993; Gilbert et al., 1995).

For myosins to support motility, a large "effective" duty ratio must be created by bringing together locally high concentrations of myosin and actin. Myosin-II accomplishes this in part by polymerizing into bipolar filaments. Myosin-I may accomplish this by cross-linking actin filaments via the ATP-insensitive actin-binding site on the myosin-I tail, creating highly concentrated actomyosin-I bundles capable of superprecipitation (Fujisaki et al., 1985). Such a condition exists in the actin-rich cell cortex where MIA is localized (Baines et al., 1995). For membrane-based myosin-I motility (Adams and Pollard, 1986), myosin-I may be concentrated at the membrane through localization sequences contained in the myosin-I tails, as suggested by the localization of myosin-I at membranes and clustering of myosin-I immunoreactivity on membrane surfaces (Hagen et al., 1986; Yonemura and Pollard, 1990; Baines et al., 1992; Baines et al., 1995).

Binding myosin-I to a specific receptor should increase the effective duty ratio by limiting the diffusion of the myosin-I away from an anchored actin filament, thus creating an environment that is similar to that found in the skeletal muscle fiber. These receptors may be (*a*) soluble proteins or protein complexes, like the binding of dynein to the dynactin complex (Lees-Miller et al., 1992), or (*b*) integral membrane proteins. Alternatively or additionally, one or more of the steps in the ATPase cycle may be strain dependent, so a load imposed on the myosin-I head could significantly slow the transition from the strong-binding AM.ADP to weak-binding AM.ATP states. Such a mechanism has been proposed for myosin-II in isometrically contracting skeletal muscle (Ferenczi et al., 1984; Ma and Taylor, 1994). In vitro force measurements will be required to determine if the duty ratio of myosin-I is force dependent (Finer et al., 1994).

To determine the number of myosin-I molecules required to support processive motility in dilute solutions, the duty ratio must be known. Our data do not provide a precise determination of the duty ratio. However, if we assume that the duty ratio for myosin-I is the same as that for myosin-II (less than 0.05) (Finer et al., 1995), significantly >20 molecules would be required for processive motility to occur. While this number is large, 20 tightly packed myosin-I molecules would occupy a surface area of < 25 nm $\times$ 25 nm (Jontes, J.A., and R.A. Milligan, personal communication).

Evolution of the Myosin ATPase Mechanism

Our transient biochemical study of a myosin isoform other than myosin-II provides an opportunity to obtain preliminary insights about the evolution of the myosin superfamily by comparing both the primary structures and the biochemical kinetics. The catalytic domains within each class of myosin indicate that the myosin-I and myosin-II classes arose before the divergence of eukaryotic phyla (Goodson and Spudich, 1993; Cheney et al., 1993). The biochemical mechanisms of myosin-I and myosin-II are as closely related to each other as the mechanisms of different members of the myosin-II family (Marston and Taylor, 1980; Ritchie et al., 1993). Therefore, it is likely that the com-

mon myosin ancestor had a chemical mechanism like present day myosin-I and myosin-II.

Remarkably, selection pressure has maintained this biochemical mechanism despite multiple rounds of gene duplication and divergence that have given rise to at least nine distinct myosin families that are characterized by relatively conserved motor domain sequences and highly divergent tail sequences (Cheney et al., 1993). Therefore, it is likely that (*a*) the other members of the myosin superfamily have similar chemical mechanisms, and (*b*) the basic mechanism of myosin-based motility (i.e., force generation by the transition from the predominant weak-binding states to the short-lived strong-binding states) is most suitable to support actin-based motility in the cell as well as in the muscle fiber. Analysis of the biochemical mechanisms of other members of the myosin superfamily will provide a more rigorous test of our hypothesis.

We thank E.W. Taylor for providing mant-ATP, M.W. Washabaugh and T.K. Harris for the use of their rapid-quench apparatus and technical advice, I.C. Baines for advice about myosin-I purification, E. De La Cruz for actin and helpful discussions, and the Pollard laboratory for technical assistance and helpful discussions.

This work was supported by a research grant from the National Institutes of Health (GM-26132) to T.D. Pollard. E.M. Ostap was supported in part by a grant from the Cancer Research Fund of the Damon Runyon-Walter Winchell Foundation Fellowship (DRG-1294).

Received for publication 11 October 1995 and in revised form 16 January 1996.

References

Adams, R.J., and T.D. Pollard. 1986. Propulsion of organelles isolated from *Acanthamoeba* along actin filaments by myosin-I. *Nature (Lond.).* 322:754–756.

Adams, R.J., and T.D. Pollard. 1989. Binding of myosin-I to membrane lipids. *Nature (Lond.).* 340:565–588.

Albanesi, J.P., J.A. Hammer, and E.D. Korn. 1983. The interaction of F-actin with phosphorylated and unphosphorylated myosin-IA and myosin-IB from *Acanthamoeba castellanii. J. Biol. Chem.* 258:176–181.

Albanesi, J.P., H. Fujisaki, and E.D. Korn. 1985. A kinetic model for the molecular basis of the contractile activity of *Acanthamoeba* myosin-IA and myosin-IB. *J. Biol. Chem.* 260:11174–11179.

Bagshaw, C.R. 1993. Muscle Contraction. Chapman and Hall, London. 154 pp.

Baines, I.C., H. Brzeska, and E.D. Korn. 1992. Differential localization of *Acanthamoeba* myosin I isoforms. *J. Cell Biol.* 119:1193–1203.

Baines, I.C., A. Corigliano-Murphy, and E.D. Korn. 1995. Quantification and localization of phosphorylated myosin-I isoforms in *Acanthamoeba castellanii. J. Cell Biol.* 130:591–603.

Bement, W.M., and M.S. Mooseker. 1995. TEDS rule: a molecular rationale for differential regulation of myosins by phosphorylation of the heavy chain head. *Cell Motil. Cytoskeleton.* 31:87–92.

Brzeska, H., T.J. Lynch, B. Martin, and E.D. Korn. 1989. The localization and sequences of the phosphorylation sites of *Acanthamoeba* myosin-I. An improved method for locating the phosphorylated amino acid. *J. Biol. Chem.* 264:19340–19348.

Chalovich, J.M., and E. Eisenberg. 1982. Inhibition of actomyosin ATPase activity by troponin-tropomyosin without blocking the binding of myosin to actin. *J. Biol. Chem.* 257:2432–2437.

Cheney, R.E., M.A. Riley, and M.S. Mooseker. 1993. Phylogenetic analysis of the myosin superfamily. *Cell Motil. Cytoskeleton.* 24:215–223.

Doberstein, S.K., and T.D. Pollard. 1992. Localization and specificity of the phospholipid and actin-binding sites on the tail of *Acanthamoeba* myosin-IC. *J. Cell Biol.* 117:1241–1249.

Doberstein, S.K., I.C. Baines, G. Weigand, E.D. Korn, and T.D. Pollard. 1993. Inhibition of contractile vacuole function *in vivo* by antibodies against myosin-I. *Nature (Lond.).* 365:841–843.

Eisenberg, E., and L.E. Greene. 1980. The relation of muscle biochemistry to muscle physiology. *Annu. Rev. Physiol.* 42:293–309.

Ferenczi, M.A., E. Homsher, and D.R. Trentham. 1984. The kinetics of magnesium adenosine triphosphate cleavage in skinned muscle fibres of the rabbit. *J. Physiol.* 352:575–599.

Finer, J.T., R.M. Simmons, and J.A. Spudich. 1994. Single myosin molecule mechanics: piconewton forces and nanometre steps. *Nature (Lond.).* 368:113–119.

Finer, J.T., A.D. Mehta, and J.A. Spudich. 1995. Characterization of single actin-myosin interactions. *Biophys. J.* 68:291–297s.

Fujisaki, H., J.P. Albanesi, and E.D. Korn. 1985. Experimental evidence for the contractile activities of *Acanthamoeba* myosin-IA and myosin-IB. *J. Biol. Chem.* 260:1183–1189.

Geeves, M.A. 1989. Dynamic interaction between actin and myosin subfragment 1 in the presence of ADP. *Biochemistry.* 28:5864–5871.

Geeves, M.A., and T.E. Jeffries. 1988. The effect of nucleotide upon a specific isomerization of actomyosin subfragment 1. *Biochem. J.* 256:41–46.

Gilbert, S.P., M.R. Webb, M. Brune, and K.A. Johnson. 1995. Pathway of processive ATP hydrolysis by kinesin. *Nature (Lond.).* 373:671–676.

Goodson, H.V., and J.A. Spudich. 1993. Molecular evolution of the myosin family: Relationship derived from comparisons of amino acid sequences. *Proc. Natl. Acad. Sci. USA.* 90:659–663.

Hagen, S.J., D.P. Kiehart, D.A. Kaiser, and T.D. Pollard. 1986. Characterization of monoclonal antibodies to *Acanthamoeba* myosin-I that cross-react with both myosin-II and low molecular weight nuclear proteins. *J. Cell Biol.* 103:2121–2128.

Hiratsuka, T. 1983. New ribose-modified fluorescent analogs of adenine and guanine nucleotides available as substrates for various enzymes. *Biochim. Biophys. Acta.* 742:496–508.

Holmes, K.C. 1995. The actomyosin interaction and its control by tropomyosin. *Biophys. J.* 68:2s–7s.

Johnson, K.A. 1986. Rapid kinetic analysis of mechanochemical ATPases. *Methods Enzymol.* 134:677–705.

Johnson, K.A., and E.W. Taylor. 1978. Intermediate states of subfragment 1 and actosubfragment 1 ATPase: reevaluation of the mechanism. *Biochemistry.* 17:3432–3442.

Jung, G., Y. Fukui, B. Martin, and J.A. Hammer III. 1993. Sequence, expression pattern, intracellular localization, and targeted disruption of the *Dictyostelium* myosin ID heavy chain isoform. *J. Biol. Chem.* 268:14981–14990.

Lees-Miller, J.P., D.M. Helfman, and T.A. Schroer. 1992. A vertebrate actin-related protein is a component of a multisubunit complex involved in microtubule-based motility. *Nature (Lond.).* 359:244–246.

Lynch, T.J., J.P. Albanesi, E.D. Korn, E.A. Robinson, B. Bowers, and H. Fujisaki. 1986. ATPase activities and actin-binding properties of subfragments of *Acanthamoeba* myosin IA. *J. Biol. Chem.* 261:17156–17162.

Lynch, T.J., H. Brzeska, I.C. Baines, and E.D. Korn. 1991. Purification of myosin I and myosin I heavy chain kinase for *Acanthamoeba castellanii. Methods Enzymol.* 196:12–23.

Ma, Y., and E.W. Taylor. 1994. Kinetic mechanism of myofibril ATPase. *Biophys. J.* 66:1542–1553.

Marston, S.B., and E.W. Taylor. 1980. Comparison of the myosin and actomyosin ATPase mechanisms of the four types of vertebrate muscles. *J. Mol. Biol.* 139:573–600.

Miyata, H., B. Bowers, and E.D. Korn. 1989. Plasma membrane association of *Acanthamoeba* myosin-I. *J. Cell Biol.* 109:1519–1528.

Pollard, T.D. 1982. Assays for myosin. *Methods Enzymol.* 85:123–130.

Pollard, T.D. 1984. Polymerization of ADP-actin. *J. Cell Biol.* 99:769–777.

Pollard, T.D., and E.D. Korn. 1972. A protein cofactor required for the actin activation of a myosin-like ATPase of *Acanthamoeba castellanii. Fed. Proc.* 31:502.

Pollard, T.D., S.K. Doberstein, and H.G. Zot. 1991. Myosin-I. *Annu. Rev. Physiol.* 53:653–681.

Press, W.H., B.P. Flannery, S.A. Teukolsky, and W.T. Vetterling. 1986. Numerical Recipes in C: The Art of Scientific Computing. Cambridge University Press, Cambridge, UK. 735 pp.

Rayment, I., H.M. Holden, M. Whittaker, C.B. Yohn, M. Lorenz, K.C. Holmes, and R.A. Milligan. 1993. Structure of the actin-myosin complex and its implications for muscle contraction. *Science (Wash. DC).* 261:58–65.

Ritchie, M.D., M.A. Geeves, S.A. Woodward, and D.J. Manstein. 1993. Kinetic characterization of a cytoplasmic myosin motor domain expressed in *Dictyostelium discoideum. Proc. Natl. Acad. Sci. USA.* 90:8619–8623.

Romberg, L., and R.D. Vale. 1993. Chemomechanical cycle of kinesin differs from that of myosin. *Nature (Lond.).* 361:168–170.

Sinard, J.H., and T.D. Pollard. 1990. *Acanthamoeba* myosin-II minifilaments assemble on a millisecond time scale with rate constants greater than those expected for a diffusion limited reaction. *J. Biol. Chem.* 265:3654–3660.

Spudich, J.A., and S. Watt. 1971. The regulation of rabbit skeletal muscle contraction. I. Biochemical studies of the interaction of the tropomyosin-troponin complex with actin and the proteolytic fragments of myosin. *J. Biol. Chem.* 246:4866–4871.

Taylor, E.W. 1991. Kinetic studies of the association and dissociation of myosin subfragment 1 and actin. *J. Biol. Chem.* 266:294–302.

Titus, M.A., D. Wessels, J.A. Spudich, and D. Soll. 1993. The unconventional myosin encoded by the *myo*A gene plays a role in *Dictyostelium* motility. *Mol. Biol. Cell.* 4:233–246.

White, H.D., and I. Rayment. 1993. Kinetic characterization of reductively methylated myosin subfragment-1. *Biochemistry.* 32:9859–9865.

Yonemura, S., and T.D. Pollard. 1990. Localization of myosin-I and myosin-II in *Acanthamoeba. J. Cell Sci.* 102:629–642.

Zot, H.G., S.K. Doberstein, and T.D. Pollard. 1992. Myosin-I moves actin filaments on a phospholipid substrate: implications for membrane targeting. *J. Cell Biol.* 116:367–376.